Applied Catalysis B: Environmental 207 (2017) 195–206

Contents lists available at ScienceDirect

Applied Catalysis B: Environmental

journal homepage: www.elsevier.com/locate/apcatb

Research Paper

Pyridinic-N groups and ultramicropore nanoreactors enhance CO_2 electrochemical reduction on porous carbon catalysts

Wanlu Li[a,c], Barbara Herkt[a,b], Mykola Seredych[a], Teresa J. Bandosz[a,c,*]

[a] Department of Chemistry and Biochemistry, The City College of New York, New York, NY 10031, USA
[b] Program in Laboratory Technology, Erhvervsakademi Aarhus Hasselager Allé 8, Viby 8260, Denmark
[c] Ph.D. Program in Chemistry, The Graduate Center of the City University of New York, New York, NY 10016 USA

ARTICLE INFO

Article history:
Received 15 September 2016
Received in revised form
13 December 2016
Accepted 6 February 2017
Available online 7 February 2017

Keywords:
N-doped nanoporous carbon
CO_2 reduction
Surface chemistry
Carbon monoxide
Methane

ABSTRACT

Wood-based activated carbons, as received and modified by introduction of nitrogen and/or oxidation, were studied as CO_2 electrochemical reduction reaction (CO_2ERR) catalysts. The carbons have similar pore structures but they differ significantly in surface chemistry. An electrochemical reduction process applied to the surface before CO_2 reduction increased their catalytic performance. On the carbons tested Faradaic efficiency for CO formation reached 40% and methane formation – 1.2% at –0.66 V vs. RHE. The high efficiency for the CO formation was linked mainly to positively charged carbon close to pyridinic nitrogen, which stabilizes $CO_2^{\bullet-}$ intermediate in the pore system. On the other hand, the results indicate that quaternary nitrogen is less influential and it is less affected by the reduction process. N-oxides outside the ring ($C—N^+—O^-$) were also found as active sites for CO_2ERR. Hydrogen evolution reaction and CO_2ERR compete for these active sites. Owing to the specific texture of nanoporous carbon, Faradaic reactions might not be a unique mechanism of CH_4 formation. It is also possible that CO, upon strong adsorption in ultramicropores of sizes less than 0.7 nm combines there with adsorbed H_2 from water reduction resulting in the formation of methane. Thus, the ultramicropores can be considered as pseudo Fisher-Tropsch nanoreactors. The results also indicate that the acidic surface of the catalysts increases the overpotential of the maximum Faradaic efficiency of either CO or CH_4 formation.

1. Introduction

CO_2 electrochemical reduction reaction (CO_2ERR) has gained a significant attention since it provides a possible solution for minimizing the CO_2 concentration level in the environment and offers an alternative way to convert it to renewable fuels. Various metals (Ag [1,2], Au [3], Cu [4–6]) and metal complexes [7,8] have been investigated as heterogeneous catalysts for CO_2 reduction. However, many polycrystalline metals show low product selectivities and high overpotentials [1,3,4]. Moreover, the rising cost of noble metals and low stability of the catalysts are the main hindrance towards their practical applications [9]. Therefore, there is a need to develop a new class of catalysts, which are less expensive than metals and sufficient for CO_2ERR.

Recently, nitrogen-doped carbon-based materials become one of the most intensively studied electrocatalysts for various processes. Wu and co-workers [10] tested nitrogen-doped carbon nanotubes for CO_2ERR. The results showed that the onset overpotential was 0.18 V with 37% Faradaic efficiency (FE) for the CO formation. Maximum FE reached 80% at a low overpotential of 0.26 V. Sharma and co-workers [11] used various nitrogen-containing precursors and heating temperatures in order to control the specific nitrogen functionalities of carbon nanotubes. They found that pyridinic-N groups are more active for the CO formation than the quaternary nitrogen. Density functional theory (DFT) calculations indicated that pyrrolic nitrogen has little influence on CO_2ERR [11]. These results contradict to those of Xu et al. [12], which showed that the intrinsic activity for CO formation correlates better with the amount of quaternary nitrogen than with the pyridinic-N. Wang and co-workers [13] reported that FE for formate on N-doped graphene reached its maximum of 73% at –0.84 V vs. RHE. That efficiency dropped to 20% in 1 h. Methane was not detected on these carbon nanostructures. Methane was reported when carbon phase worked as a support for catalytic phases such as metals [14], metal oxides [15], or organometallic compounds [16]. Varela and co-workers [16] studied the carbon blacks functionalized with nitrogen and Mn and/or Fe ions. Except CO formation (FE

* Corresponding author at: Department of Chemistry and Biochemistry, The City College of New York, New York, NY 10031, USA.
E-mail address: tbandosz@ccny.cuny.edu (T.J. Bandosz).

http://dx.doi.org/10.1016/j.apcatb.2017.02.023
0926-3373/

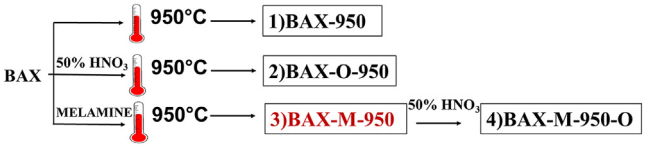

Scheme 1. A schematic summary of the treatments applied to initial BAX carbon.

80% at −0.5 V vs. RHE at 10 min), methane was found on Fe containing catalysts. It was concluded that strong CO–metal interactions on iron sites drive the reduction reaction. A recent review on electrochemical reduction of CO_2 on carbon materials does not report CH_4 formation on pure carbon electrodes [17]. Nevertheless, it indicates that a high surface area or their nanofibrillar structure, high electrical conductivity, positively charged carbon atoms, a high work function of carbon nanofibers, or low free energy for CO_2 activation, high barrier for H_2 evolution and high binding energies of the intermediate complexes generated are significant assets of carbon catalysts during CO_2 electroreduction reaction.

Besides nanostructured carbon such as nanotubes or graphene, porous carbons can also offer a great potential for catalytic applications. An important and unique asset is their developed surface area. To improve the electronic/catalytic features of porous carbons, nitrogen heteroatoms are incorporated to a carbon matrix using various N-containing precursors (such as melamine, urea, polyaniline, *etc.*) [18,19] or by reactions of a carbon matrix with NH_3 or amines [20]. The speciation of nitrogen functionalities depends both on the nature of N- containing precursors and on the temperature of carbonization/heat treatment [21]. At relatively low temperatures (400–700 °C) mainly amides, amines and cyano groups dominate on the carbon surface. After a high temperature treatment (>700 °C) nitrogen tends to exist in the forms of pyridine, quaternary nitrogen, pyrrole and pyridine-N-oxide. Since pyridinic and quaternary nitrogen in carbon-based materials were found to be active for CO_2 electrochemical reduction [10–13,22], nitrogen incorporation at a high temperature is expected to be the most beneficial to improve the properties of carbons as catalysts.

In our recently reported results on CO_2 electroreduction on dual-doped (S- and N-) nanoporous derived from polymers we have shown that the catalytic performance was governed by the positively charged sites in the carbon matrix. There was an indication that pyridinic-N brought a positive charge to the neighboring carbon atoms and stabilized $CO_2^{\bullet}-$/*COOH intermediate, which are important steps for the CO formation [22]. Besides, the surface basicity and high volume of ultramicropores improved the CO_2 reduction process. The results also suggested that the porosity might be crucial for the CH_4 formation. Even though we generally suggested the mechanism, the specific catalytic role of nitrogen groups in CO_2ERR needs further investigation. Therefore, the objective of this paper is to develop a more comprehensive view on the CO_2 electroreduction in a confined space of carbon nanopores whose surface is decorated with well-defined nitrogen species. The overall acidity/basicity, porous structure, and the changes in the surface features of catalysts caused by HER and CO_2ERR are extensively studied. Based on the trends, the specific mechanism is proposed.

2. Experimental procedures

2.1. Materials

A wood-based commercial activated carbon BAX-1500 (Mead Westvaco), which is referred to as BAX was chosen for this study. Scheme 1 shows the treatments applied to this carbon: 1) Heating to 950 °C (10 °C/min) followed by 30 min holding at this temperature (under N_2). The obtained sample is referred to as BAX-950. 2) Oxidizing with 50% HNO_3 for 5 h at room temperature, and then washing in a Soxhlet apparatus to remove the excess of the oxidizing agent and water-soluble compounds. This process was followed by the treatment at 950 °C as described in Procedure 1. This sample is referred to as BAX-O-950. 3) Soaking in a melamine suspension (mass ratio = 1.5:1) in ethanol for 5 h under stirring at room temperature. The mixture was then boiled until the evaporation of the alcohol and dried at 120 °C. As the next step, the sample was heated at 950 °C as in the treatment Procedure 1. This carbon is referred to as BAX-M-950. 4) The latter sample was then further oxidized with 50% HNO_3 and followed by the treatment Procedure 2. This sample is referred to as BAX-M-950-O.

2.2. Methods

2.2.1. CO_2 electrochemical reduction

To prepare a working electrode, a homogeneous slurry of an active material with polyvinylidene fluoride (PVDF) and carbon black (8:1:1) in N-methyl-2-pyrrolidone (NMP) was prepared, and then coated double sides onto a Ti foil (1 cm^2). Eventually, a uniform 5 ± 0.2 mg/cm^2 catalyst loading was obtained. Such prepared electrodes were dried at 100 °C overnight in an oven. At the target potential (0.66 V vs. RHE), the current density for Ti foil is 0.196 mA/cm^2, which is an order of magnitude less than on our catalysts. Taking into account this, and the fact that the titanium foil was fully covered by the layer of the catalyst, we assumed that current generated on Ti does not affect our results in a marked way.

The CO_2ERR was evaluated at different reduction potentials in CO_2 (ultrapure) saturated $KHCO_3$ electrolyte (0.1 M) on VersaSTAT MC (AMETEK, Princeton Applied Research). The test was performed in an airtight three-electrode and two compartments cell separated by a cation exchange membrane (Nafion 117). Ag/AgCl/NaCl (3 M) was used as a reference electrode and Pt wire as a counter electrode. The potentials were corrected taking into account the measured Ohmic drop. Before the electrochemical CO_2 reduction reaction, the electrodes were wetted in $KHCO_3$ (0.1 M) for 4 h with an open circuit potential (OCP) vs. Ag/AgCl was recorded. Then the cyclic voltammetry (CV) experiments were run in the potential window from 0 V to −1.5 V vs. Ag/AgCl (0.74 V to −0.76 V RHE after Ohmic drop) to test the stability with an increase in the number of cycles. The OCP and CV measurements were performed in the N_2-saturated electrolyte. Potential values are reported versus reversible hydrogen electrode (RHE): E (vs. RHE) = E (vs. Ag/AgCl) + 0.21 V + 0.059 × pH (pH of saturated CO_2 0.1 M $KHCO_3$ is 6.8). Initially, linear sweep voltammograms were obtained in N_2 or CO_2 saturated electrolyte in the potential range from 0.04 V to −1.06 V vs. RHE at a scan rate of 5 mV/s. To evaluate the performance of CO_2ERR, the electrolyte was purged with CO_2 for 30 min and headspace of the cell for 20 min. Then the chronoamperometry (CA) was run under constant potentials for 6 h between −0.36 V and −1.06 V vs. RHE. During the CA run, the gas phase products from the headspace of the cathodic compartment of the electrochemical cell were analyzed every hour using gas chromatograph (GC) (model SRI 8610C). The gas phase was injected into the GC column using a gastight syringe and the separation was done on a carboxen column (Carboxen-1000, 4.57 m in length, and 2.1 mm in internal diameter). The GC oven heating program was as follows: 35 °C for 5 min, then heating from 35 to 220 °C at a rate of 20 °C/min and holding at 220 °C for 5 min. The carrier gas was He with a flow rate of 30 mL/min. A flame ionization detector (FID) was used to detect hydrocarbons, and a thermal conductivity detector (TCD) to detect CO. CO and CH_4 were the target reduction products. Even though the concentration of CH_4 was very small, it was in the range of the amount used to calibrate the detector (R^2 = 0.992). To account for all the charge delivered to the system, on the best performing sam-

ple the detection of hydrogen was carried out using TCD and argon as a carrier gas. Additionally the content of the electrolyte solution after CO_2ERR was tested using NMR. ^{1}H NMR data were acquired at 298 K on a Bruker 800 MHz Advance III HD spectrometer equipped with a 5-mm TCI cryoprobe. 1D ^{1}H NMR spectra were recorded with a sweep of 16 ppm centered on the water, 1.7 s acquisition time, 2 s relaxation delay, gradient excitation sculpting water suppression, for the total of 512 scans.

In order to study the effect of reduction process on the efficiency of CO_2ERR, the active electrode material was reduced in a N_2 saturated electrolyte at the constant potential −0.66 V vs. RHE for 4 h in a chronoamperometry (CA) mode. After this CA pretreatment, the active electrode materials are referred to with an additional letter "R" added after their names. Then these electrode samples were directly either exposed to CO_2 applying CA for 48 h (referred to with "CO_2" added to their names) or to N_2 in the electrolyte applying CA for 48 h (referred to with letter "S") at the potential −0.66 V vs RHE. The former test was done to evaluate the stability of CO_2ERR process and the latter test was done to evaluate the stability of the carbon matrix itself.

2.2.2. Characterization of the catalysts

2.2.2.1. Sorption of nitrogen. Sorption of nitrogen was measured on ASAP 2020 Surface Area and Porosity Analyzer (Micromeritics) at −196 °C. Before each analysis, the samples were outgassed at 120 °C to constant vacuum (10^{-4} Torr). At these conditions only physically adsorbed species were removed without changing the surface chemistry. From the isotherms, the surface areas (BET method), total pore volumes (V_t), the volumes of mesopore (V_{meso}), micropore (V_{mic}), ultramicropore ($V_{<0.7nm}$) and the volume of pores smaller than 1 nm ($V_{<1nm}$), were calculated. The pore size distributions were calculated using the Non-Linear Density Functional Theory (NLDFT) (www.nldft.com) [23].

2.2.2.2. Potentiometric titration. Potentiometric titration analysis was carried out on a DMS Titrando 888 automatic titrator (Metrohm). The samples (∼0.050 g) were added to 25 mL of $NaNO_3$ (0.01 M), and equilibrated overnight at room temperature. The suspension was saturated with N_2 throughout the measurements under a continuous stirring to eliminate the influence of atmospheric CO_2. Each sample was titrated with base after adding 0.1 M HCl to the sample suspension. Volumetric standard NaOH (0.1 M) was used as a titrant. The experimental data were transformed into a proton binding curves, Q, and then to pK_a distributions. The latter was done using SAIEUS numerical procedure [23,24]. The initial pH of the suspension was discussed as the surface pH value.

2.2.2.3. X-ray photoelectron spectroscopy (XPS). The XPS data were collected in the Physical Electronics PHI 5000 VersaProbe II spectrometer with a monochromatic Al Kα radiation (50 W, 15 kV, 1486.6 eV). Prior to analysis, all samples were outgassed until 10^{-8} Torr at room temperature. High-resolution spectra of powdered samples were detected with the constant pass energy values of 29.35 eV and a 200 μm diameter analysis area at a take-off angle of 45°, whilst 117.4 eV pass energy was used for the survey spectra and the calculation of surface atomic concentration. The spectrometer energy scale was calibrated using Cu $2p_{3/2}$, Ag $3d_{5/2}$, and Au $4f_{7/2}$ photoelectron lines at 932.7, 368.3, and 84.0 eV, respectively. The SmartSoft-VP2.6.3.4 software package was used for acquisition and data analysis and Multipack software was used to fit photoelectron spectra. A Shirley-type background was subtracted from the signals. Recorded spectra were fitted using Gauss–Lorentz curves in order to determine the binding energy of the different element core levels accurately.

3. Results and discussion

3.1. CO_2 electrochemical reduction activity

The electrocatalytic performance of N-doped BAX-M-950 and it oxidized counterpart, BAX-M-950-O was studied first. After stabilization of the active electrode materials under N_2, linear sweep voltammetry (LSV) (Fig. 1a) experiments were carried out in the presence or absence of CO_2 in the 0.1 M $KHCO_3$ electrolyte. The current density in the N_2-saturated electrolyte is attributed to the hydrogen evolution reaction (HER) and capacitive behavior. The current density increment in the CO_2-saturated electrolyte at more negative potentials could indicate that the CO_2 reduction reaction took place in addition to HER. This occurred at −0.60 V vs. RHE for BAX-M-950 and at −0.92 V vs. RHE for BAX-M-950-O. However, an increase in the current density is not a conclusive evidence for CO_2 reduction since it might be due to the decreasing pH (from 8.34 to 6.80) [25] in the electrolyte after saturation with CO_2. Therefore, to further support the CO_2 reduction a direct evidence for the formation of reduction products is needed.

The formation of CO and CH_4 during CO_2ERR was tested by cathodic headspace sampling at various potentials during the chronoamperometry experiments (CA). The examples of gas chromatograms are presented in Fig. S1 of Supplementary Information. It is worth mentioning that the intensity of the peak corresponding to oxygen remained the same during CO_2ERR and its origin is from air. CO was the main reaction product of CO_2ERR. The trends in FE for CO and CH_4 at various potentials calculated at 4 h reduction process are shown in Fig. 1c and 1d. Both BAX-M-950 and BAX-M-950-O catalyzed CO formation starting at −0.36 V vs. RHE, corresponding to the overpotential of 0.25 V. The potential at which the specific product was first detected was considered as the onset potential. The onset potential for the N-doped wood-based carbon is shifted to the more positive value comparing to the dual-doped (S- and N-) polymer-derived carbon (−0.59 V vs. RHE) studied previously [22]. BAX-M-950 reached the maximum FE of about 24% at −0.66 V vs. RHE and then it decreased at more negative potentials. The decrease suggests that at negative potentials hydrogen evolution reaction (HER) is more dominant than that of CO_2 reduction reaction. Interestingly CH_4 was formed and FE of its formation at different potentials showed a similar trend to that for CO. The best performance was at more negative potential than that for CO (−0.76 V vs. RHE) with FE of 0.75%. The oxidized sample BAX-M-950-O showed similar maximum of FE for CO (25%) and CH_4 (0.79%), however, the highest FEs were found at more negative potentials than those for BAX-M-950.

To study the stability of the catalysts during CO_2ERR, BAX-M-950 was chosen and its electrochemical performance was tested at −0.66 V for 24 h. Fig. 2 shows that FE for CO and CH_4 changes with time. For CO, FE increased from 16% to 24% at the first 4 h (increased 50%) and then decreased gradually to 15% after 24 h. The current density maintained at a steady value (1.4 mA/cm^2) throughout the test. For CH_4, the trend of FE differs from that for CO and it kept increasing and reached 0.7% after 24 h. The marked increase in FE for CO formation up to 4 h could be due to the kinetics of the mass transport of CO_2 to the surface of electrode, slow CO release from the surface, or some changes in surface chemistry of the active electrode material during reduction, which are beneficial for the CO formation.

To investigate the reason of the increased FE with the reduction time, a reduction pretreatment in N_2 was applied for 4 h at the potential −0.66 V vs. RHE before CO_2ERR. Interestingly, after this reduction process on BAX-M-950, the FEs for both CO and CH_4 increased significantly and reached 40% (1 h) and 1.2% (6 h), respectively (Fig. 2). An FE for CO formation was still observed an increase with the reduction time (increased 3% in 1 h) but the increase was

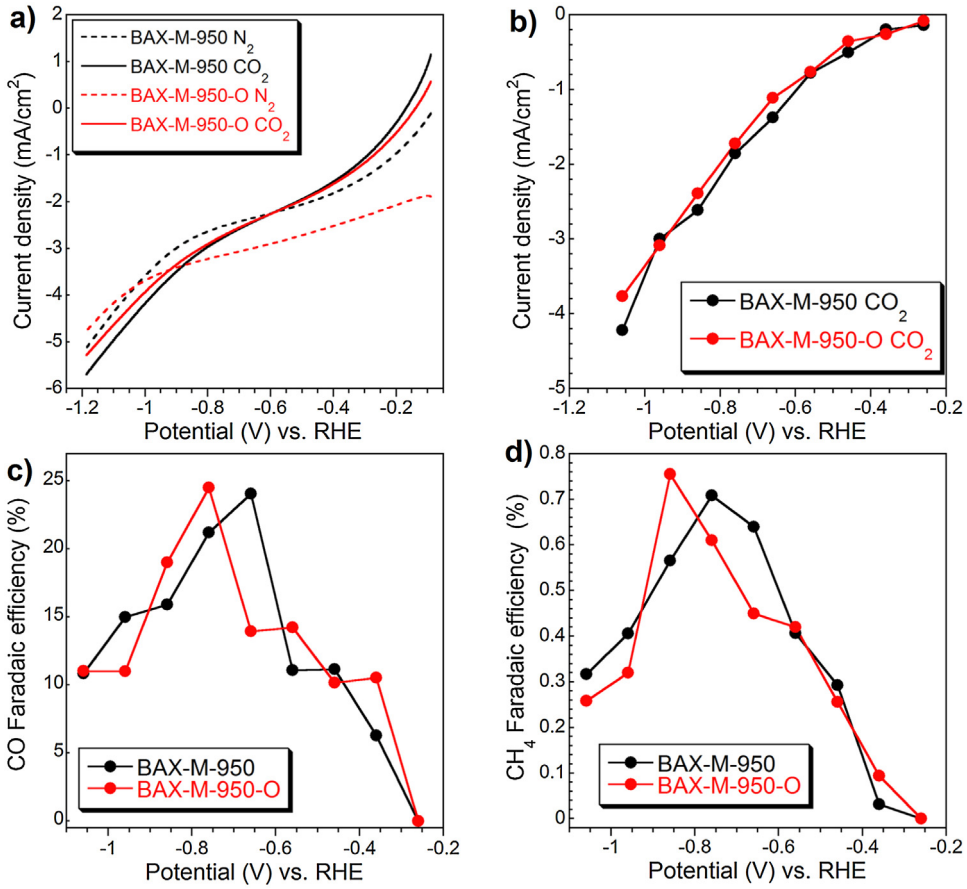

Fig. 1. a) LSV in the N_2 and CO_2 saturated electrolyte in 0.1 M $KHCO_3$ for BAX-M-950 and BAX-M-950-O; b) Stationary CO_2 electrochemical reduction current density for BAX-M-950 and BAX-M-950-O; Faradaic efficiency of CO c) and CH_4 formation d).

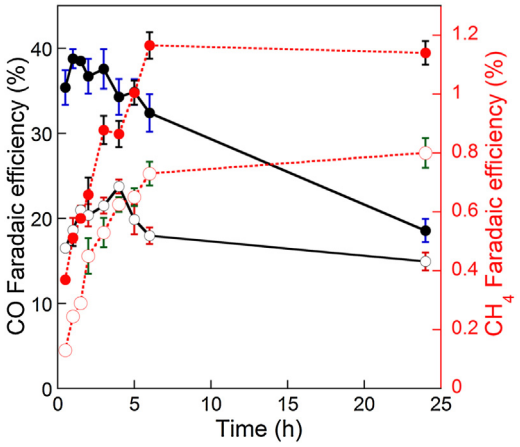

Fig. 2. Faradaic efficiency for CO (solid black lines) and CH_4 (dashed red lines) formation at the potential −0.66 V vs. RHE with (solid dots) and without (hollow dots) the reduction pretreatment (in N_2) for BAX-M-950. (For interpretation of the references to colour in this figure legend, the reader is referred to the web version of this article.)

smaller than that before the reduction pretreatment. Therefore, under the same mass transport conditions, the marked FE differences before and after the reduction of BAX-M-950 in N_2 indicate that the reduction pretreatment process of the catalysts favors the CO_2 reduction.

The electrochemical performance of reduced BAX-M-950 in CO_2 was compared to those of other carbons tested after the reduction pretreatment in N_2. The results are collected in Fig. 3a and b. BAX-950 showed a very poor Faradaic efficiency for the catalytic conversion CO_2 to either CO or CH_4, while BAX-M-950 showed the best performance for CO. It is interesting that at the beginning of the CO_2ERR process (6 h) BAX-O-950 and BAX-M-950 exhibit a similar FE for CH_4 formation. BAX-M-950-O showed a lower FE for CH_4 than did BAX-O-950 and BAX-M-950 after 3 h of CO_2ERR process. Fig. 3c displays the comparison of CO FE after 1 h of the reduction process and CH_4 FE after 6 h of reduction. At these conditions, BAX-M-950 exhibited the best performance with FE for CO of 40% and for CH_4 of 1.2%, respectively. Following this, the amount of CH_4 formed was compared to the amount of CO detected after 24 h of CO_2ERR (Fig. 3d). A linear trend between the amounts of CH_4 and CO suggests that the formation of CH_4 is linked to the amount of CO formed on the carbon surface.

Since the carbon catalysts could decompose/undergo chemical reactions during the electrochemical reduction process, especially at more negative potentials, we tested those materials for the release of both CO and CH_4 after reduction pretreatment at −0.66 V vs. RHE without CO_2 in the electrolyte. The electrolyte was saturated with nitrogen. The highest amount of CO (FE of 0.5%) was released from the surface of BAX-O-950 starting from 6 h (Fig. 4a). For BAX-M-950, which showed the best performance for CO_2 reduction, CO was detected after 48 h with FE of 0.2%. The trace amounts of CH_4 were detected in the case of all N-doped activated carbons through the whole electrochemical process (Fig. 4b). It is important to mention that the amounts of CO and CH_4 released from the carbons during the reduction under N_2 were almost negligible compared to those detected during CO_2ERR. This indicates the good stability of our carbon catalysts under the reduction conditions.

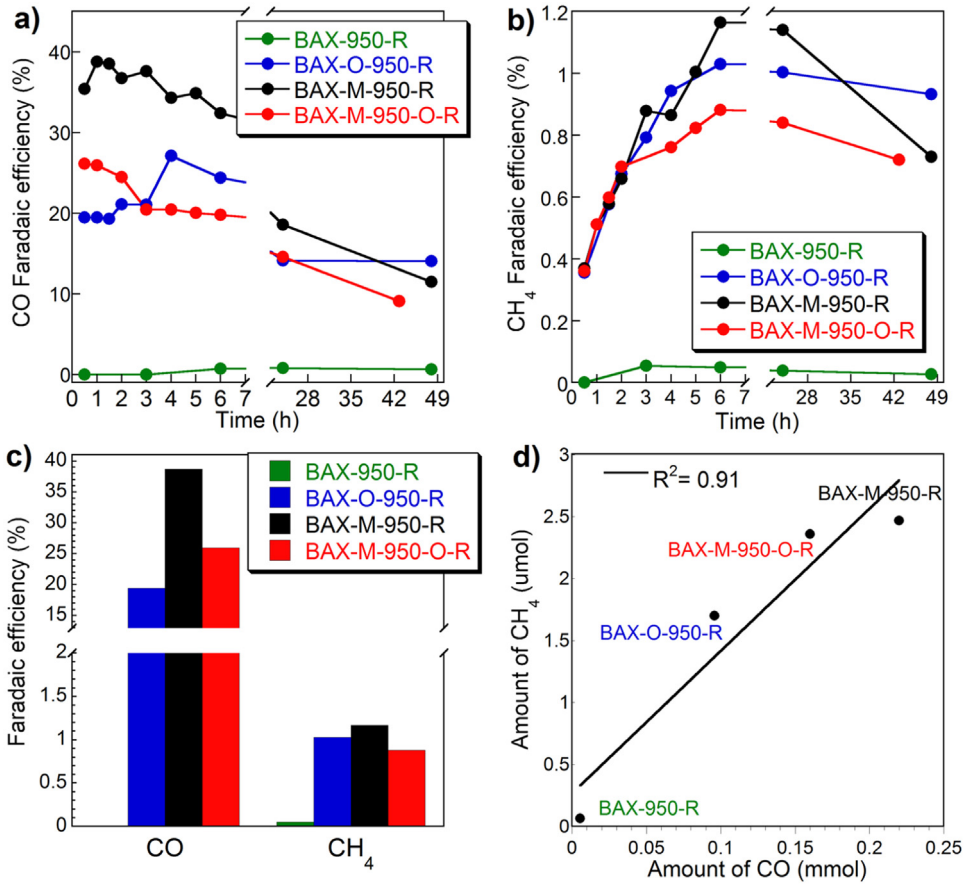

Fig. 3. a) Faradaic efficiency for CO and b) CH_4 formation during CO_2 reduction at the potential −0.66 V vs. RHE after reduction pretreatment in N_2; c) The comparison of the CO FEs for the materials studied at the potential of the best performance of BAX-M-950; d) The dependence of the amount of CH_4 formed on the amount of CO formed (after 24 h of CO_2 reduction) for all the carbons studied.

The current densities in the presence or absence of CO_2 are compared at −0.66 V vs. RHE (Fig. 4c). The differences in the current densities in CO_2 and N_2 saturated electrolytes are linked to the catalytic activity of carbon toward CO_2ERR. As shown in Fig. 4c, the biggest difference is observed for BAX-M-950, which is consistent with the trends in FE for the reduction products.

To account for all current delivered to the system, the extent of hydrogen evolution was tested on the best preforming initial and reduction pretreated BAX-M-950 sample. The summary of the Faradaic efficiencies is presented in Fig. 5. As seen, the total Faradaic efficiency is 85% after 48 h reduction for pretreated BAX-M-950. H_2 and CO are the major products and the pretreatment only slight increased the efficiency for HER. Based on the results collected, we cannot account for 15% of Faradaic efficiency. Taking into account the specificity of our system it could be due to the following reasons: 1) Since BAX-M-950 exhibits a capacitance of 92 F g^{-1} in a 0.1 M $KHCO_3$ electrolyte (potential window 0.74 V to −0.76 V vs. RHE) some charge is stored in the pore system of the carbon; 2) Owing to the high porosity of the catalysts some products could be adsorbed in the pores and therefore are not detected in the headspace; 3) Some products could be dissolved in the electrolyte. Since owing to the small amount of carbon we are not able to test hypothesis 2 at this stage, to test hypothesis 3 NMR analysis of the electrolyte after CO_2 reduction was carried out. The ^{1}H NMR spectra are presented in Fig.S2 of Supplementary information. Trace amount of formic acid and methanol in the solution were detected. The amounts of these products was not evaluated precisely since this work focuses on the detection of CO and CH_4. Nevertheless, these results help us to account for the current delivered to the system and support the results discussed above.

3.2. Characterization of the catalysts

To account for the differences in the catalytic performance, the surfaces of the carbons were studied in details from the points of view of their texture and chemistry. The parameters of the porous structure are presented in Table 1. All BAX carbons are micro/mesoporous (Fig. 5) and 38–54% of the total pore volume exists in micropores. The treatment with melamine followed by a high temperature heating increased the volume of ultramicropores as a result of a partial gasification of the carbon and removal of carbon atoms from the pore walls caused by the incorporation of nitrogen groups to the carbon matrix. This development of microporosity might positively affect the efficiency for CO_2 electrochemical reduction. Interestingly, in spite of the similar volumes of ultramicropores in BAX-M-950-O and BAX-M-950 their electrochemical performance in CO_2 differs and the latter sample outperforms the former one at −0.66 V vs. RHE (Fig. 1). This suggests that the ultramicroporosity is not a predominant factor affecting the electrochemical reduction of CO_2. The difference in the performance might be also related to the incorporation of oxygen containing groups or oxidation of reduced nitrogen in micropores as a result of HNO_3 treatment. Such changes in chemistry, besides affecting the catalytic activity, can also block the pores for CO_2 molecules limiting their access to the catalytic centers. Another reason affecting the apparent activity of our carbons might be in the ash content, which is about 4.5% in BAX-950. The main constituent

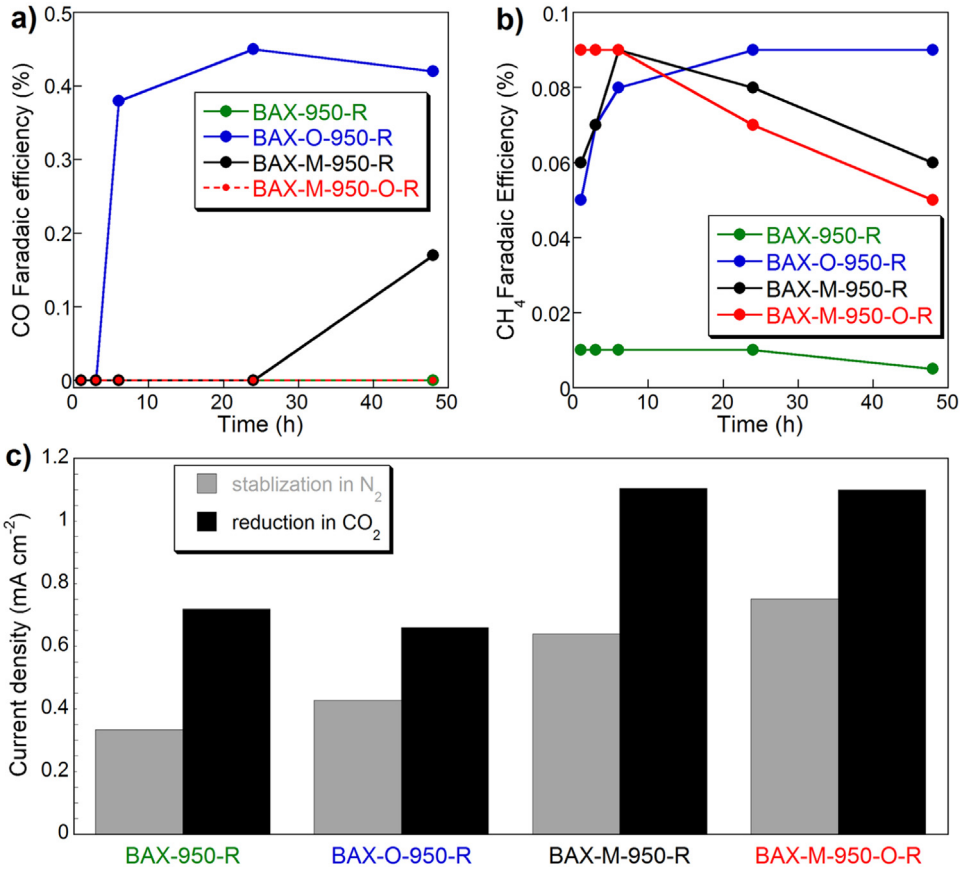

Fig. 4. Faradaic efficiency for a) CO and b) CH_4 formation in N_2-saturated electrolyte after reduction pretreatment in N_2 (R) at the potential −0.66 V vs. RHE and c) The comparison of the current densities in N_2 and CO_2 saturated electrolyte at the potential −0.66 V vs. RHE.

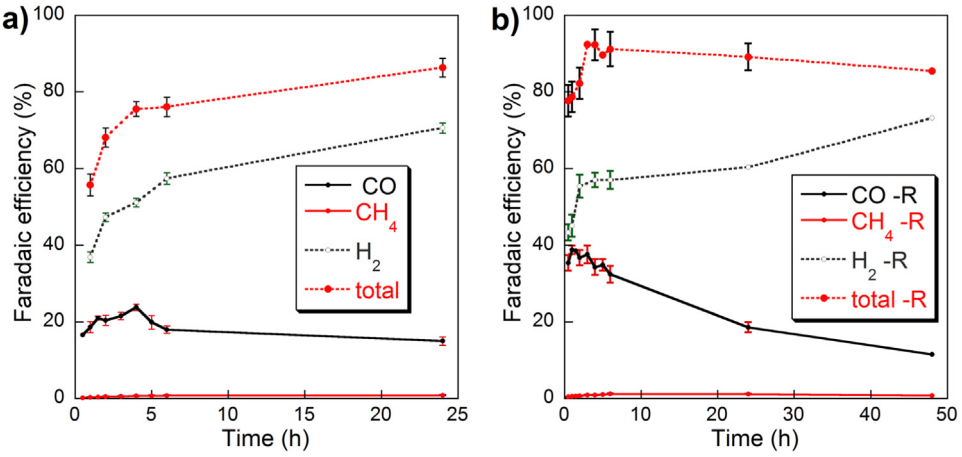

Fig. 5. FE for formation of CO, CH_4 and H_2 on the initial BAX-M-950 sample (a) and reduction pretreated counterpart (b).

Table 1
The parameters of the porous structure for the materials studied.

Sample	S_{BET} (m^2/g)	V_t (cm^3/g)	V_{meso} (cm^3/g)	$V_{<0.7nm}$ (cm^3/g)	$V_{<1nm}$ (cm^3/g)	V_{mic} (cm^3/g)	V_{mic}/V_t
BAX-950	1533	0.951	0.509	0.110	0.201	0.442	0.46
BAX-O-950	1404	0.811	0.377	0.084	0.207	0.434	0.54
BAX-M-950	1494	1.032	0.637	0.146	0.195	0.395	0.38
BAX-M-950-O	1440	0.995	0.611	0.145	0.198	0.384	0.39

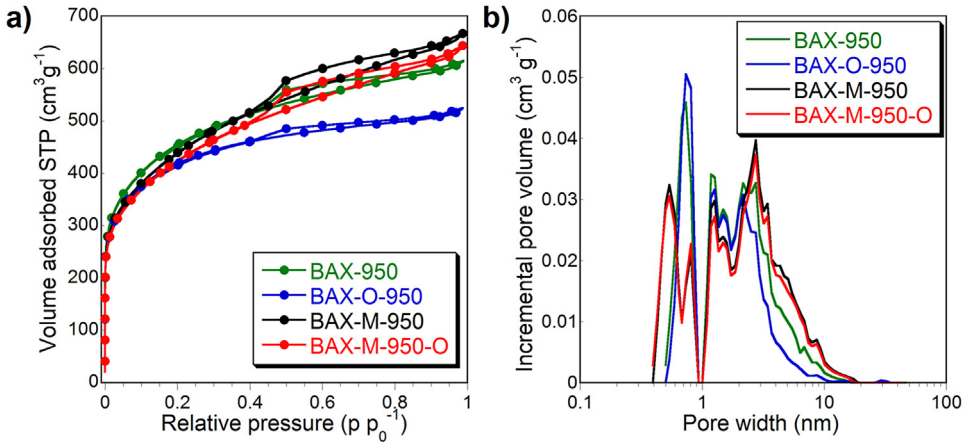

Fig. 6. a) Nitrogen adsorption isotherms at −196 °C and b) Pore size distributions for the materials studied.

of ash in wood based carbons are silica and iron oxides in the fraction of percent (<0.1%) [26,27]. As indicated by Lum et al. [14], Chua *et al.* [15], Varela et al. [16], even a small amount of a metal based phase can affect the mechanism of the catalytic process. Although the acid treatment is expected to decrease the content of metal impurities, and thus might decrease the amount of metals catalyzing CO_2 reduction on our carbons, if this process indeed takes place, a counter argument against the role of ash is a very low catalytic activity on BAX-950-R (Fig. 4 a and b). The results suggest that however CO_2ERR is not directly related to the porosity, it seems that the surface chemistry in those pores might be crucial for the electrochemical conversion of CO_2 to CO. Nevertheless, the maximum values of FEs for CH_4 and CO reduction on BAX-M-950-O and BAX-M-950 are very similar in spite of the fact that the potential at which it happens is more favorable on the latter sample. It is also important to mention, that based on PSDs (Fig. 5b) those two carbons have the smallest pores (∼0.5 nm) among all carbons tested. Thus the strong adsorption of reactants in the pores should not be neglected in analyzing the mechanism of CO_2 reduction. This process should take place in very small ultramicropores (less than 0.7 nm), where in fact the functional groups should not be present due to their bulky structure.

In order to evaluate the influence of acidity/basicity of the catalysts on CO_2ERR, the surfaces of the initial carbons were studied using the potentiometric titration. Table 2 summarizes the distributions of the acidity constants for the species present on the carbons' surfaces along with pH values. Proton binding curves and pK_a distributions are presented in the Supplementary Information (Fig. S3). BAX-950, BAX-O-950 and BAX-M-950 have similar surface pH values since the majority of oxygen containing groups (carboxylic acids, lactone and anhydride) was expected to decompose at 950 °C [28]. As anticipated, the oxidation of BAX-M-950 results in a significant increase in its acidity, which is due to twice more total acidic groups on the surface than those on BAX-M-950 itself. This might be related to the presence of nitro-type complexes (pK_a 9–10) and carboxylic groups (pK_a 4–5) [29].

Linking the electrochemical performance to surface acidity shows that formation of CO and CH_4 on the acidic N-doped carbon BAX-M-950-O occurs at higher overpotentials than on neutral BAX-M-950 (Fig. 1c and d). The acidic carbon also showed highest current density in the N_2-saturated electrolyte (Fig. 4c), which indicates the most intense process for HER. These results suggest that the electrochemical reduction of CO_2 is less favorable on an acidic surface, which is also consistent with the results of our previous study that acidic surface of carbon enhanced HER [22].

XPS analysis was performed on the initial carbons, on the active electrode materials after reduction pretreatment in N_2 for 4 h (R), on the carbons reduced in N_2 for 48 h at the potential −0.66 V vs. RHE (S), and on the carbons exposed to CO_2 at the potential −0.66 V vs. RHE (CO_2). Comparing the initial samples, for BAX-M-950 (Fig. 7c), an increase in the content of nitrogen was found in comparison to BAX-950 (Fig. 7b). Interestingly, oxidation of BAX with HNO_3 followed by the heat treatment also resulted in an incorporation of some nitrogen groups into the carbon matrix. Even though BAX-M-950 and BAX-M-950-O (Fig. 6d) have a similar content of nitrogen, the oxidation process increases the content of oxygen dramatically and leads to the acidic nature of the latter carbon, as discussed above. Interestingly, except for the oxidized N-doped carbon (BAX-M-950-O), after reduction pretreatment in N_2 either during 4 h (R) or 48 h (S) at the potential of −0.66 V vs. RHE a slight decrease in the oxygen content is found (Fig. 7). After CO_2 reduction slightly more oxygen was introduced to the surface of all N-doped carbons in comparison to the amount after the pretreatment processes in N_2-saturated electrolyte. Even though the results suggest that our carbons work as electrocatalysts, the small increase in the oxygen content after CO_2ERR could be related to the oxidation of the carbon surface by the byproduct of CO_2 reduction, mainly by the released oxygen during the CH_4 formation [30]. The oxidation of some sites can be a limiting factor for these catalyst applications. At this stage an important observation is that an increase in the surface oxygen content after of CO_2ERR is in fact very small and by all means not comparable to that found for S and N-co-doped carbons [22].

Since based only on the content of elements it is rather impossible to explain the differences in the performance of our materials, the detailed deconvolution of C 1*s*, O 1*s*, N 1*s* core energy level spectra was carried out (Table S2, Fig. S4–S7 of Supplementary Information). The deconvolution of C 1*s* core energy level spectra (Table S2) show that melamine treated carbons have more carbon atoms involved either in C—O or C—N bonds than has BAX-950. The deconvolution of N 1*s* core energy level spectra (Table S2) clearly shows that the most oxidized nitrogen is in BAX-M-950-O. Both BAX-M-950 and BAX-M-950-O have similar distributions of nitrogen in pyridines and pyrroles/pyridones but the latter sample has nitric oxides (nitro-type complexes NO_2). This species are the results of the treatment with nitric acid [31]. Nitrogen in BAX-O-950 (Fig. S5) is only in pyridines and pyridones/pyrroles but their contributions are much smaller than those in the melamine treated samples.

The pervious researches indicated that pyridinic-N and quaternary-N were crucial for CO_2 electroreduction [10–13,22].

Table 2
Surface pH values, peak positions and numbers of groups (in parentheses, [mmol/g]) for the material studied.

Sample	Surface pH	pK_a 4–5	pK_a 5–6	pK_a 6–7	pK_a 7–8	pK_a 8–9	pK_a 9–10	pK_a 10–11	All
BAX-950	7.35	4.05 (0.074)	5.37 (0.045)	6.71 (0.106)	7.57 (0.088)		9.14 (0.112)	10.31 (0.233)	0.658
BAX-O-950	7.29	4.04 (0.086)	5.29 (0.038)	6.24 (0.051)	7.17 (0.085)	8.64 (0.115)		10.00 (0.214)	0.588
BAX-M-950	7.39	4.45 (0.094)	5.59 (0.039)	6.60 (0.084)	7.84 (0.088)		9.34 (0.154)	10.41 (0.051)	0.510
BAX-M-950-O	5.83	4.34 (0.137)	5.31 (0.080)	6.65 (0.115)	7.88 (0.091)		9.33 (0.208)	10.41 (0.270)	0.901

Our results also show that BAX-M-950 has more of those groups than have the other carbons tested, which likely results in its higher FE of the CO and CH_4 formations. Interestingly, even though BAX-M-950 and BAX-M-950-O have the similar contents of pyridinic-N (N-6) and quaternary-N (N-Q) moieties, and similar volumes of ultramicropores, the former sample shows the better electrochemical performance. This can be linked to its less acidic surface, as discussed above. The relationship between the pyridinic-N content and their FE for CO formation is illustrated in Fig. 8. Interestingly, a linear trend is found for the carbons having neutral pH. BAX-M-950-O does not follow the trend since its acidic surface favors HER. However, no trend is found between the electrochemical performance and the amount of quaternary-N. This observation provides direct evidence that the content of pyridinic-N is more influential than quaternary-N for CO_2ERR especially with regard to the CO formation.

In the analysis of O 1*s* and N 1*s* core energy level spectra (Supplementary Information, Table S5) for the initial carbons and those treated in various conditions we focus first on the best performing N-doped carbon, BAX-M-950. To find out why the reduction pretreatment improves the CO_2 reduction performance, the results of the XPS analysis of the samples after the reduction pretreatment process in N_2 at −0.66 V vs. RHE were compared to those of the initial carbons (Fig. 9). Indeed, it was found that the surface groups were reduced after this process. The deconvolution of C 1*s* shows that O—C=O and carbonate/occluded CO groups were reduced to carbonyl/quinone (C=O), and to phenolic/alcoholic/etheric (C—O) species. This is supported by the deconvolution of O 1 *s* core energy level spectra which shows that the C—O groups were reduced to C=O. The deconvolution of N 1*s* indicates that there is a small increase in the pyridinic-N and quaternary-N after the reduction process in N_2. Therefore, the observed enhancement in the performance is likely due to the effect of the more reducing surface environment. This process could also increase the small pore accessibility for CO_2. Unfortunately, due to the very small weight of the electrode active material its porosity cannot be evaluated.

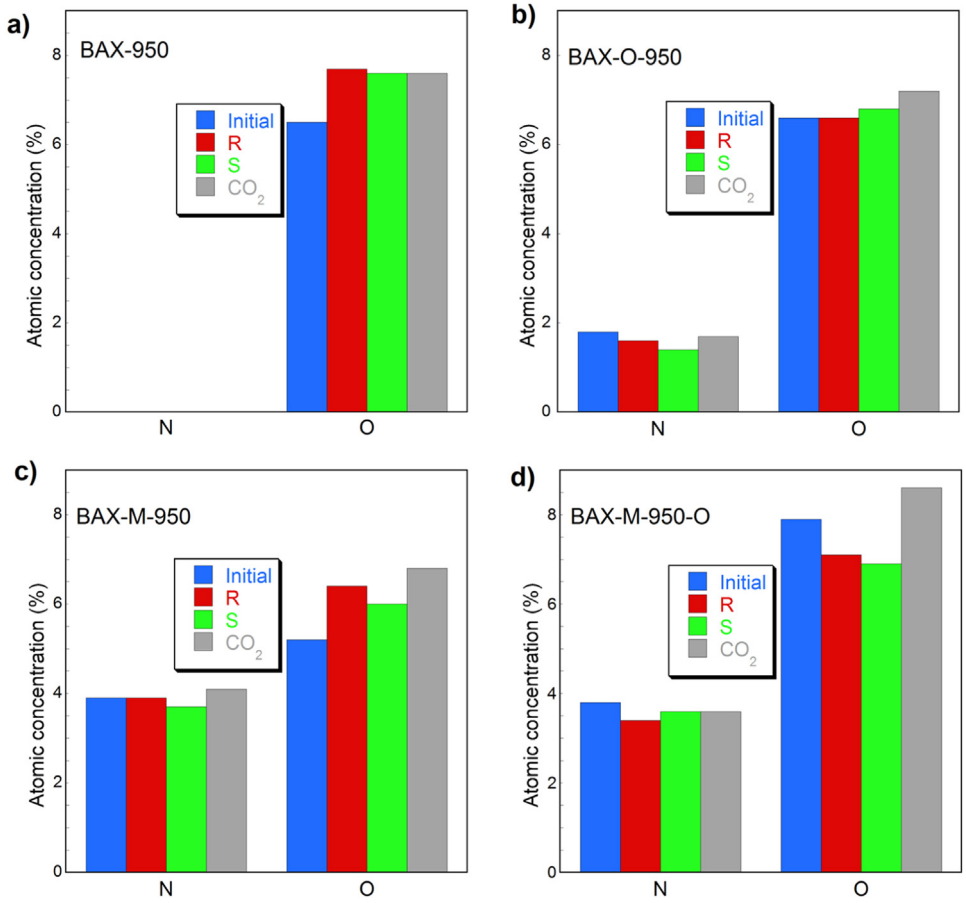

Fig. 7. Atomic concentration of nitrogen and oxygen for initial carbons, on the active electrode materials after reduction pretreatment in N_2 for 4 h (R), on the carbons reduced in N_2 for 48 h (S), and exposed to CO_2 for 48 h (CO_2) at the potential −0.66 V vs. RHE.

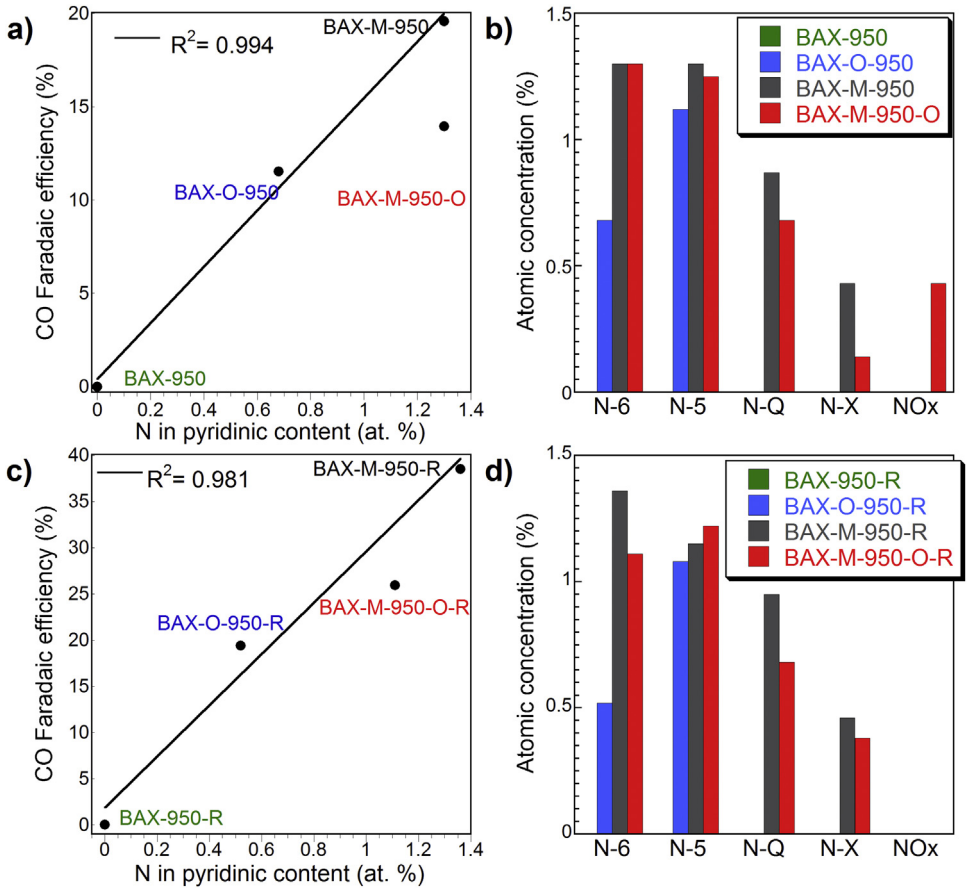

Fig. 8. a) The Faradaic efficiency for CO formation (1 h) as a function of the content of pyridinic-N in the initial carbons; b) Atomic concentration of the nitrogen groups for the initial carbons; c) The Faradaic efficiency for CO formation (1 h) as a function content of pyridinic-N for the reduction pretreated nanoporous carbons (R); d) Atomic concentration of the nitrogen groups for the reduction pretreated carbons (R).

Chronoamperometry run in N_2-saturated electrolyte for 48 h results in hydrogen evolution from water reduction. For BAX-M-950, the XPS results (Supplementary Information, Table S5) show that the configurations of carbon and oxygen species remain basically the same. However, there are obvious changes in the nitrogen species. The contributions of the pyrroles/pyridones (N-5) groups increased. This is accompanied by a decrease in the contribution of pyridine-N oxides (N-X). It should be noted that nitrogen in pyrrolic-N and pyridonic-N have similar binding energies and therefore the XPS analysis cannot distinguish between them. Nitrogen in pyrrolic groups is expected to be electrochemically stable since the lone pair on nitrogen atom is in the *p* orbital so it is involved in the 6π electron aromatic system [32]. Therefore, the increase in the contribution at the binding energy of 401.5 eV corresponds to the pyridonic-N species. One of their sources can be the reduction of pyridine-N-oxides at the applied potential [33]. It is worth to mention that the reduction pretreatment during 4 h (BAX-M-950-R) at the potential −0.66 V vs. RHE did not affect the amount of pyridine N-oxides, which indicates that the reduction of these species needs a longer exposure to reducing environment or higher overpotential. Since pyridine-N-oxides were reduced by the applied potential after 48 h (BAX-M-950-S), they cannot be considered as the active sites for CO_2ERR. These findings are also consistent with that of Kumar and co-workers [33] The XPS analysis clearly shows that the amounts of nitrogen groups in the form of pyridinic quaternary nitrogen decreased more after electrochemical reduction of CO_2 for BAX-M-950 compared to those for the pretreated sample (BAX-M-950-R), which indicates their activity for CO_2ERR.

BAX-O-950 reduction, either in N_2 or CO_2 saturated electrolyte, resulted in a decrease in pyridinic-N, which was accompanied by an increase in pyridonic-N (Fig. 9a). Since on BAX-O-950 pyridine-N-oxides are not detected, the increase in the contribution of pyridonic-N might be of another origin. In pyridinic-N configuration, which is present on BAX-O-950, the lone pair from nitrogen is not a part of aromatic ring and thus it results in a slightly positive charge on the neighboring carbon. Therefore, formation of pyridonic-N species could be caused by oxidation of that positively charged carbon and in this process pyridone groups could be formed. Also a decrease in the contribution of pyridinic-N in the N_2-saturated electrolyte indicates (BAX-O-950-R and BAX-O-950-S) that HER consumes pyridinic-N. Zheng et al. [34,35] suggested that pyridinic-N is one of the active sites that favor hydrogen evolution. Thus, HER and CO_2ERR compete with each other for the pyridinic-N active sites.

The XPS analysis of BAX-M-950-O indicates that there are NO_x species on the initial sample. After the 4 h reduction pretreatment (BAX-M-950-O-R), NO_x groups were entirely reduced to a $C{-}N^+{-}O^-$ (N-X) form. Interestingly, after 48 h of CO_2 reduction (BAX-M-950-CO_2), most of $C{-}N^+{-}O^-$ was consumed and further oxidized to NO_x, which also indicates that the structure of N-oxides outside of carbon ring ($C{-}N^+{-}O^-$) could also be the active site for CO_2 reduction.

3.3. Proposed mechanism

The XPS results on the samples exposed to the N_2-saturated electrolyte (R) were compared to those exposed to the CO_2-

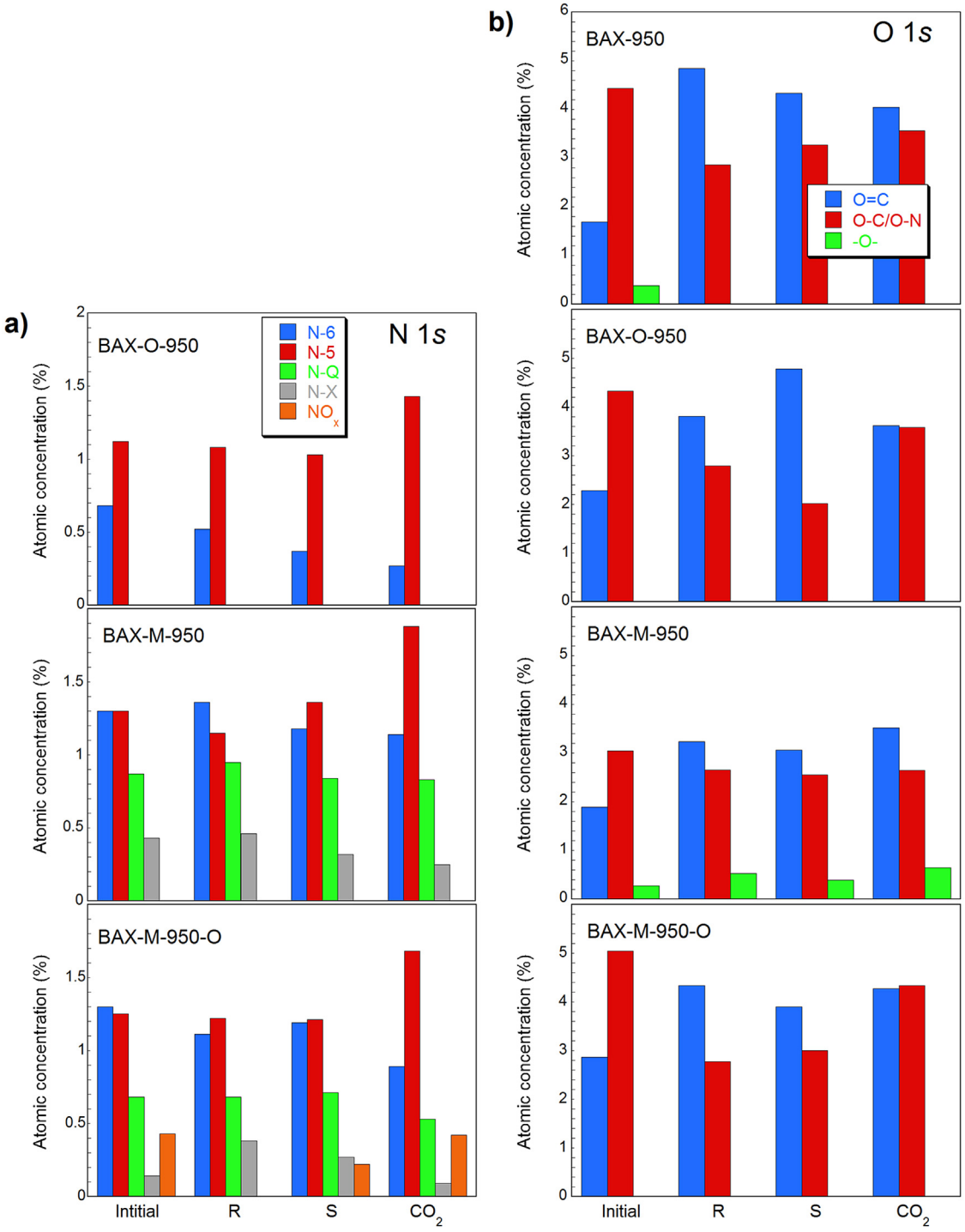

Fig. 9. Comparison of atomic concentration for the specific oxygen and nitrogen groups. (R-samples after 4 h pretreatment in N_2; S-samples after 48 h reduction in N_2 after the pretreatment; CO_2–samples after 48 h reduction in CO_2 after the pretreatment).

saturated electrolyte (CO_2). The results collected clearly showed that pyridine-N is the most active sites in the reduction process. N-oxides outside of the ring (C—N^+—O^-) were also found as active sites, which provide the intrinsic activity for CO_2ERR. Our previous findings also support the results collected [22]. We have proposed that the negatively charged intermediate $CO_2^{\bullet-}$is stabilized on the positively charged sites introduced into the carbon matrices as a result of heteroatom doping. Then the intermediate is further reduced to CO through accepting electrons from the cathodic current. CO is released and a part of it is re-adsorbed in the small pores. The new results suggest that the cathodic current itself plays a role in the reduction of the carbon surface. Long CO_2ERR gradually causes oxidation the pyridinic-N and C—N^+—O^- groups by oxygen released from CO_2 molecule. 48 h of the reduction process did not diminish the catalytic activity of the surface groups since CO_2 reduction still took place. The amount of CH_4 formed depends on the amount of CO adsorbed in the system. In addition, the HER evolution competes with CO_2ERR for the pyridinic-N sites in the aqueous electrolyte. The surface acidity favors the pro-

tonation process and thus can further deplete the active sites for CO_2ERR.

There are no reports on the CH_4 formation on N-doped CNTs or fibers [10–12]. These materials,contrary to the carbons used in our research, are nonporous. Provided that the chemical active sites located in the pore system predominantly participate in the CO formation, its adsorption seems to be an important step for methane formation. These pores, owing to small sizes and thus a high adsorption potential, bind CO strongly. On the other hand, N-doped CNT or fibers will not produce any methane since weakly adsorbed CO will desorb before further reduction can take place. Nevertheless, due to the porous nature of our carbon the methane formation might not be an exclusively electrochemical process. As mentioned above, both BAX-M-950 and BAX-M-950-O have similar FE for CH_4 formation in spite of some differences in surface chemistries. Based on their almost identical sizes and volumes of ultramicropores, we hypothesize that these pores, owing to the strong adsorption potential, attract/trap some formed CO and act as Fisher-Tropsch nanoreactors. The classical Fisher-Tropsch process consists of the following steps, which take place in a chronological order: 1) an associative adsorption of CO; 2) splitting of the C—O bond 3) dissociative adsorption of two hydrogen molecule; 4) transferring of two hydrogen atoms to the oxygen to yield H_2O; 5) desorption of H_2O; 6) transferring of two hydrogen atoms to the carbon atom to yield CH_2 [36]. According to Beguin and coworkers [37] at negative potentials porous carbons show the capability to store hydrogen from the water reduction process. Hydrogen molecule, owing to its very small size (2.89 Å) should be attracted to the same ultramicropores where CO is adsorbed. Therefore, in confined space and under high pressure, a coexistence of CO and H_2 might result in formation of methane and water. Strong CO adsorption should promote C—O bond splitting. Even though CH_4 can be a byproduct in the classical Fisher-Tropsch process, its formation there is undesirable. In our system, owing to the small sizes of pores/nanoreactors, large hydrocarbons are rather not formed. Another pseudo Fisher-Tropsch scenario, which also has a high probability to take place in our electrochemical system, is related to attraction of H^+ ions to the carbon surface in small pores [37] where *CO is adsorbed. In such a case the dissociative splitting of hydrogen is not needed and carbon reduction and protonation take place simultaneously. To prove this hypothesis further experiments with CO adsorption are planned but their scope is beyond the objective of this paper. It is also important to mention here that the apparent performance of carbon catalysts might include the complex effect of ash. Although in the discussion of the results we have excluded its predominant role in the reduction process, it is always present in inexpensive carbons obtained from a biomass or coal. If nanoporous carbons perform well as CO_2 reduction catalysts, the final efficiency should be a driving force for their catalytic application. In fact, if in some carbons ash is found catalytically active, its presence should be considered only as an advantage since an expensive impregnation with metals or other catalytic phases would not be needed.

4. Conclusions

The results presented in this paper show that the melamine-treated carbon is the best electrocatalyst for CO_2 reduction with the FE for CO and CH_4 formation reaching 24.2% and 0.75% at the −0.66 V vs. RHE and −0.76 V vs. RHE, respectively. The performance of the carbon catalysts dramatically increased upon their reduction in N_2 at the potential −0.66 V vs. RHE for 4 h. After this pretreatment process CO was formed with FE 40% and CH_4 with 1.2% at their maxima. The mechanism of CO_2ERR is attributed to the positively charged sites introduced into the carbon matrix. It was observed that besides pyridinic and quaternary-type nitrogen configurations, N-oxides outside the ring (C—N^+—O^-) are also active sites for CO_2ERR. Hydrogen evolution reaction and CO_2ERR compete for these sites. The linear correlation between the amounts of the pyridinic-N and the FE of CO formation indicates the predominant role of these species in the CO_2ERR process. This study also implies that the acidic surface increases the overpotential for the maximum FE of the CO formation and promotes HER. The porosity of the carbons was found to play an important role not only for improving CO_2 interactions with the surface but also for the CO retention. It is proposed that CO, when adsorbed in ultramicropores, combines with hydrogen molecule from water reduction forming methane. Such system, owing to confined pore space, works as pseudo Fisher-Tropsch nanoreactors.

Acknowledgments

The NSF collaborative CBET Grant No. 1133112 supported this work. The authors thank N. A. Travlou for her help with preparing BAX-M-950 and BAX-M-950-O samples. ^{1}H NMR data presented herein were collected in part at the City University of New York Advanced Science Research Center (CUNY ASRC), Biomolecular NMR Facility

Appendix A. Supplementary data

Supplementary data associated with this article can be found, in the online version, at http://dx.doi.org/10.1016/j.apcatb.2017.02.023.

References

[1] B.A. Rosen, A. Salehi-Khojin, M.R. Thorson, W. Zhu, D.T. Whipple, P.J.A. Kenis, R.I. Masel, Science 334 (2011) 643–644.
[2] Q. Lu, J. Rosen, Y. Zhou, G.S. Hutchings, Y.C. Kimmel, J.G. Chen, F. Jiao, Nat. Commun. 5 (2014) 3242.
[3] Y. Hori, A. Murata, K. Kikuchi, S. Suzuki, J. Chem, Soc. Chem. Commun. (1987) 728–729.
[4] Y. Hori, A. Murata, R. Takahashi, J. Chem. Soc. Trans. 85 (1989) 2309–2326.
[5] C.W. Li, M.W. Kanan, J. Am. Chem.Soc. 134 (2012) 7231–7234.
[6] M. Gattrell, N. Gupta, A. Co, Chemistry 594 (2006) 1–19.
[7] E. Simón-Manso, C.P. Kubiak, Organometallics 24 (2005) 96–102.
[8] M.R. DuBois, D.L. DuBois, Acc. Chem. Res. 42 (2009) 1974–1982.
[9] Y. Li, Q. Sun, Adv. Energy Mater. (2016) 1600463.
[10] J. Wu, R.M. Yadav, M. Liu, P.P. Sharma, C.S. Tiwary, L. Ma, X. Zou, X.D. Zhou, B.I. Yakobson, J. Lou, et al., ACS Nano 5 (2015) 5364–5371.
[11] P.P. Sharma, J. Wu, R.M. Yadav, M. Liu, C.J. Wright, C.S. Tiwary, B.I. Yakobson, J. Lou, P.M. Ajayan, X.D. Zhou (Eds.), Chemie. – Int. Ed. 54 (2015) 13701–13705.
[12] J. Xu, Y. Kan, R. Huang, B. Zhang, B. Wang, K.H. Wu, Y. Lin, X. Sun, Q. Li, G. Centi, et al., ChemSusChem 9 (2016) 1085–1089.
[13] H. Wang, Y. Chen, X. Hou, C. Ma, T. Tan, Green Chem. 18 (2016) 3250–3256.
[14] Y. Lum, Y. Kwon, P. Lobaccaro, L. Chen, E.L. Clark, A.T. Bell, J.W. Ager, ACS Catal. 6 (2016) 202–209.
[15] C.K. Chua, Z. Sofer, B. Khezri, R.D. Webstera, M. Pumera, Phys. Chem. Chem. Phys. 18 (2016) 17875–17880.
[16] A.S. Varela, N.R. Sahraie, J. Steinberg, W. Ju, H. Oh, P. Strasser, Angew. Chem. Int. Ed. 54 (2015) 1–6.
[17] S.R. Yang, X. Waldvogel, A.C.S. Jiang, ACS Appl. Mater. Interfaces 8 (2016) 28357–28371.
[18] N.P. Wickramaratne, M. Jaroniec, Adsorption 20 (2014) 287–293.
[19] B. Qiu, C. Pan, W. Qian, Y. Peng, L. Qiu, F. Yan, J. Mater, Chem. A 1 (2013) 6373–6378.
[20] M.S. Shafeeyan, W.M.A.W. Daud, A. Houshmand, A. Shamiri, J. Anal, Appl. Pyrolysis 89 (2010) 143–151.
[21] M. Seredych, D. Hulicova-Jurcakova, G.Q. Lu, T.J. Bandosz, Carbon 46 (2008) 1475–1488.
[22] W. Li, M. Seredych, E. Rodríguez-Castellón, T.J. Bandosz, ChemSusChem 9 (2016) 606–616.
[23] J. Jagiełło, T.J. Bandosz, J.A. Schwarz, Carbon 32 (1994) 1026–1028.
[24] J. Jagiello, J.P. Olivier, Adsorption 19 (2013) 777–783.
[25] M. Ma, K. Djanashvili, W.A. Smith (Eds.), Angew. Chemie - Int. 55 (2016) 6680–6684.
[26] C. Petit, T.J. Bandosz, Microporous Mesoporous Mater. 114 (2008) 137–147.
[27] S. Bashkova, A. Bagreev, T.J. Bandosz, Catal. Today 99 (2005) 323–328.
[28] T.J. Bandosz, C.O. Ania, Surface chemistry of activated carbons and its characterization, in: T.J. Bandosz (Ed.), Interface Science and Technology, Elsevier, Oxford, 2006, pp. 159–229.

[29] G. Kortum, W. Vogel, K. Andrussow, Dissociation Constants of Organic Acids in Aqueous Solution, Butterworth, London, 1961.
[30] X. Nie, M.R. Esopi, M.J. Janik, A. Asthagiri, Angew. Chemie – Int. Ed. 52 (2013) 2459–2462.
[31] C. Moreno-Castilla, M.A. Ferro-Garcia, J.P. Joly, I. Bautista-Toledo, F. Carrasco-Marín, J. Rivera-Utrilla, Langmuir 11 (1995) 4386–4392.
[32] G. Dryhurst, Pyrrolesa, Porphyrins, Electrochemistry of Biological Molecules, in: G. Dryhurst (Ed.), Elsevier, Oxford, 1977, pp. 392–472.
[33] B. Kumar, M. Asadi, D. Pisasale, S. Sinha-Ray, B.A. Rosen, R. Haasch, J. Abiade, A. L.Yarin, A. Salehi-Khojin, Nat. Commun. 4 (2013) 2819–2826.
[34] Y. Zheng, Y. Jiao, Y. Zhu, L.H. Li, Y. Han, Y. Chen, A. Du, M. Jaroniec, S.Z. Qiao, Nat. Commun. 5 (2014) 1–8.
[35] Y. Zheng, Y. Jiao, L.H. Li, T. Xing, Y. Chen, M. Jaroniec, S.Z. Qiao, ACS Nano 8 (2014) 5290–5296.
[36] H. Schulz, Appl Catal A. Gen. 186 (1999) 3–12.
[37] K. Jurewicz, E. Frackowiak, F. Béguin, A. Appl. Phys. 78 (2004) 981–987.